 https://doi.org/10.3311/PPci.38869

Periodica Polytechnica Civil Engineering, 69(3), pp. 838–849, 2025

Experimental Investigation on the Dynamic Characteristics of Representative Sand and Clay in the Beijing Region

Ye Cheng[1,2], Jinghu Yang[1,2*]

[1] Emergency Science Research Institute, Chinese Institute of Coal Science, no. 5, Qingnian Gou Road, Chaoyang District, 100013 Beijing, P.R. China
[2] Tian Di Science & Technology Co., Ltd Beijing technology research branch, no. 5, Qingnian Gou Road, Chaoyang District, 100013 Beijing, China
[*] Corresponding author, e-mail: yjh_cumtb@126.com

Received: 25 November 2024, Accepted: 04 May 2025, Published online: 21 May 2025

Abstract

In order to gain a more accurate understanding of the dynamic characteristics of soil, vibration triaxial tests were conducted on representative sand and clay samples from the Beijing area. The study investigated the influence of varying loading frequencies, cyclic stress ratios, and confining pressures on soil strength and liquefaction resistance, while also analyzing changes in shear modulus and damping ratio. The dynamic shear modulus of both sand and clay decreases with increasing shear strain, with higher confining pressures resulting in larger shear moduli. For sand, the damping ratio decreases as shear strain increases; however, for clay it initially increases before decreasing. Overall, clay exhibits a larger dynamic shear modulus but smaller damping ratio compared to sand. The number of cycles experienced by both sand and clay samples decreases with increasing confining pressure or deviational stress. As loading frequency increases, the number of cycles gradually rises for sand samples but first increases then decreases for clay samples. The damping ratio of sand gradually declines with an increase in cycle count while that of clay remains relatively stable. The variations observed in shear modulus and damping ratio are influenced by factors such as loading frequency, confining pressure, and deviating stress.

Keywords

vibration triaxial test, dynamic characteristics, pore water pressure, shear modulus, damping ratio, representative soil

1 Introduction

Soil dynamic characteristics are the key parameters in geotechnical seismic engineering and seismic design. Their spatial variability significantly influences surface motion amplification, foundation liquefaction, and the dynamic response of underground structures. However, in complex sedimentary alluvial plain regions (e.g., Beijing), traditional empirical models struggle to accurately capture the nonlinear dynamic behavior of heterogeneous soils [1]. As a rapidly expanding megacity, Beijing faces the challenge of triple dynamic coupling: the multi-layer sandy soil-clay deposition within the Cenozoic faulted basin forms a geological structure characterized by "rigid-flexible interlayers"; the dense subway network induces spatio-temporal superposition effects of vibration loads. These factors pose potential seismic risks to super high-rise building complexes in the Beijing-Tianjin-Hebei Seismic Belt [2]. Existing homogeneous soil dynamic models, such as the equivalent linear method, exhibit prediction errors of up to 40% for the seismic response spectrum at typical sites in Beijing, severely limiting the enhancement of urban lifeline resilience [3].

The dynamic shear modulus and damping ratio are critical parameters for characterizing the dynamic behavior of cohesive soil, directly influencing the nonlinearity of soil response and seismic stability analysis of a site [4, 5]. Research indicates that the dynamic characteristics of various soils are governed by multiple factors: Li [6] demonstrated that frequency significantly affects the dynamic shear modulus and damping ratio of clay but has a weaker influence on sandy soil. Yang [7] highlighted that soil burial depth is positively correlated with the dynamic elastic modulus and negatively correlated with the damping ratio. Wang [8] verified that the dynamic shear modulus of saturated loess is lower than that of unsaturated loess,

Cite this article as: Cheng, Y., Yang, J. "Experimental Investigation on the Dynamic Characteristics of Representative Sand and Clay in the Beijing Region", Periodica Polytechnica Civil Engineering, 69(3), pp. 838–849, 2025. https://doi.org/10.3311/PPci.38869

whereas its damping ratio is higher. Zhao [9] elucidated that the moisture content of fill soil is inversely related to dynamic parameters, while compaction degree is positively correlated with the maximum shear modulus and negatively correlated with the damping ratio; these parameters exhibit mild variations within the frequency range of 1–4 Hz. The Thakur [10] study further revealed that the shear modulus of low-plasticity clay decreases with increasing strain, whereas the damping ratio shows little sensitivity to strain changes.

Soil liquefaction is one of the primary causes of secondary earthquake-induced disasters [11]. Accurately understanding the evolution of soil properties during the liquefaction process holds substantial research significance and practical value for addressing the issue of large deformation in liquefied soils [12]. Acceleration plays a critical role in altering the motion state of particles [13], as high-frequency vibrations can lead to the degradation of particle material structures, thereby reducing shear stress [14]. The development of liquefaction is significantly influenced by loading path dependence [15]. A reduction in soil particle size exhibits a strong negative correlation with liquefaction potential, while anti-liquefaction strength decreases markedly with increasing strain levels [16]. Nicolas and Alain [17] classify the motion of sand into three distinct categories: under an acceleration amplitude of less than 1g, sand exhibits vibrational compression; when the acceleration amplitude approaches 1 g, particles on the sand's free surface demonstrate flow behavior; and for an acceleration amplitude exceeding 1 g, convection and stratification occur within the sand. At the same relative density, anti-liquefaction strength increases with confining pressure. However, at lower relative densities, even if confining pressure is substantially reduced, anti-liquefaction strength remains stable up to a certain limit [18]. Shan [19] demonstrated that bonding failure facilitates particle sliding and rolling, which fundamentally explains the disparity in energy dissipation between pure sand and sand-clay mixtures.

Furthermore, numerous scholars have conducted extensive research on the dynamic shear modulus and damping ratio of representative surface soil in various regions across China [20–26]. Confining pressure plays a crucial role in the liquefaction of sandy soil, whereas the influence of sandy soil itself is relatively limited under subway vibration [27]. However, there is limited research on the liquefaction failure behavior of typical sand and clay in Beijing under dynamic loading conditions, as well as insufficient reports on the evolution of soil shear modulus and damping ratio during cyclic loading.

In this study, a systematic investigation was carried out on the unique engineering geological conditions in the Beijing area. This study was deemed necessary due to scientific gaps in three key dimensions: First, the complex sedimentary structure formed by the intersection of the Yongding River alluvial fan and the Chaobai River alluvial fan poses challenges for traditional borehole sampling methods to accurately characterize the abrupt changes in dynamic parameters at the meter scale. Second, the cross-interference between subway vibrations (0.5–80 Hz) and seismic waves (0.1–10 Hz) in the frequency domain remains inadequately explained within the existing theoretical framework of soil dynamics. Most importantly, the strain-hardening behavior of Yongdinghe sand, which contains 75% silica, deviates from conventional liquefaction criteria. To achieve a more precise understanding of soil dynamics, vibration triaxial tests were performed on representative sand and clay samples collected from Beijing. The effects of varying loading frequencies, cyclic stress ratios, and confining pressures on soil strength and liquefaction resistance were systematically examined. Furthermore, the variation patterns of shear modulus and damping ratio during cyclic loading were analyzed. These research findings hold significant reference value for comprehending the dynamic characteristics of soil and enhancing its strength and liquefaction resistance.

2 Sample preparation and test method

The GDS dynamic triaxial test system, as illustrated in Fig. 1, was employed for experimental loading. It had a maximum confining pressure of 2 MPa, an axial force loading range of 0 to 10 kN, and a maximum loading frequency of 2 Hz. The prepared sample for the test was cylindrical with dimensions of diameter: 38 mm and

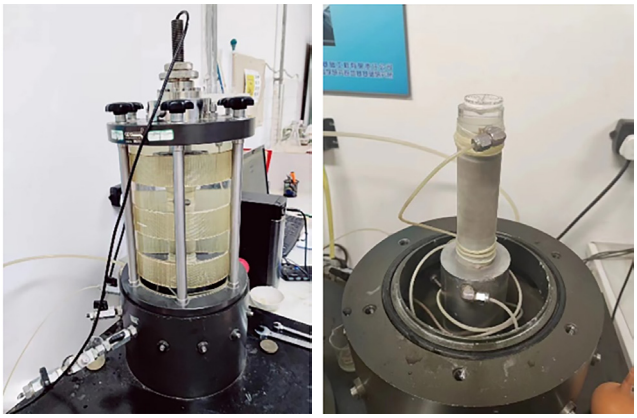

(a) (b)

Fig. 1 GDS vibration triaxial test system (a) triaxial test system, (b) specimen

height: 76 mm. This apparatus simultaneously satisfies the requirements for both triaxial shear testing and vibration triaxial testing.

The soil samples for testing were divided into clay and sand samples, which were collected from the surface sediment in the Beijing area. All sand samples were prepared using the same type of sand, as illustrated in Fig. 2 which displays the grading of the sand. Based on the gradation curve, approximately 35.3% of particles have a size greater than 0.25 mm, while about 82.3% have a size greater than 0.075 mm, indicating a medium-fine sand classification. In the clay soil sample, more than 60% of particles are smaller than 0.075 mm, with a liquid limit of 30.2%, plastic limit of 21.3%, plasticity index of 8.9, suggesting silty clay characteristics. In the triaxial test, the rubber film surrounding the sample functions as both an isolator and a pressure transmitter. During the drainage test, under confining pressure, the rubber film tends to embed into the porous structure of coarse soil, thereby affecting accurate measurement of drainage volume. However, in the sand soil test conducted in this experiment, the coarse-grained soil content did not exceed 16%, and the gradation was uniform, as evidenced by a non-uniformity coefficient of less than 5 and a curvature coefficient ranging from approximately 1 to 3. These characteristics effectively minimized the non-uniformity of the pore structure in the sand soil. Furthermore, the test utilized a film with a thickness of 0.2 mm, which significantly mitigated the film's penetration effect.

The sand and clay samples were prepared using dry density control techniques. During the sample preparation process, the dry density of the specimen was carefully controlled to be 1.73. To facilitate the preparation and molding of the sample, it was initially prepared with a moisture content of 6%, resulting in a wet density of 1.834 during this stage. Sample preparation was conducted in strict compliance with the requirements outlined in the "Standard for geotechnical test methods." The mass of the sample was determined based on its volume. To ensure uniformity in sample preparation, the specimen was divided into five distinct layers for sequential loading. Each layer was filled and compacted in accordance with the specified soil sample mass, ensuring consistent loading heights across all layers. Additionally, the contact surfaces between layers were roughened by scratching to promote better interlayer adhesion. Once the sample preparation was completed, it underwent vacuum saturation for over 12 h in a saturator device. Following this step, reverse pressure saturation was carried out by placing the sample in a loading container until reaching a pore pressure coefficient $B > 0.95$, indicating successful saturation achievement. After achieving full saturation, consolidation under predetermined confining pressure conditions took place for a duration of 2 to 4 h before proceeding with further load application according to the test plan.

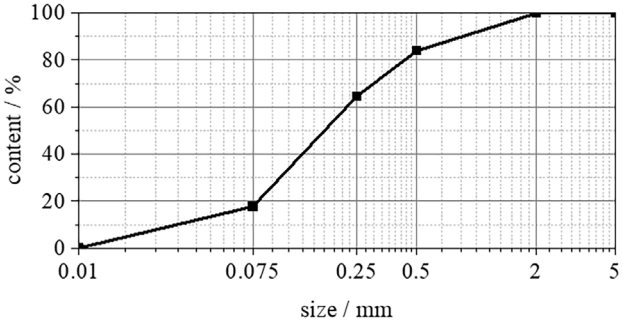

Fig. 2 Gradation curve of sand

The vibration triaxial test was conducted on a total of 20 soil samples, comprising 10 sand samples and 10 clay samples, respectively. Each soil sample was further divided into two categories: dynamic triaxial tests under graded loading and dynamic triaxial tests under cyclic loading. The case numbers of all 20 samples and their corresponding loading conditions are provided in Table 1. To save space, the samples within the same group have been combined. For instance, TS1-TS3 represent three samples subjected to confining pressures of 25, 50, and 100 kPa respectively. The loading frequency (f) ranged from 0.5 Hz to 2 Hz, while the confining pressure (p_c) varied between 25 kPa, 50 kPa, and 100 kPa. Additionally, the cyclic stress ratio ($r_{cs} = p_d/\sigma_3$) was set at values of 0.5, 1, and 2.

Fig. 3 shows the diagram of stress path during step loading, in which Fig. 3 (a) is the deviational stress (p_d) and Fig. 3 (b) is the effective stress ($p' = (\sigma_1 + \sigma_3)/2$). In the step loading test, partial stresses were incrementally increased in stages of every 5 kPa with each stage consisting of ten cycles of loading until the cumulative axial strain reached a threshold value of up to 10%. On the other hand, in the cyclic loading test, continuous loading with fixed bias stress was applied until reaching an axial strain level of up to 10%. Subsequently, the testing process was terminated.

3 Analysis of test results

Based on the vibration triaxial test of the sample, this study analyzed its dynamic characteristics and liquefaction behavior under cyclic loading. The fractional loading test was conducted to investigate the dynamic shear

Table 1 Vibration triaxial test cases

Case number	specimen	confining pressure / kPa	cyclic stress ratio	loading frequency /Hz
TS1~TS3	sand	25、50、100	step loading	1
TS4~TS6	sand	50	1	0.5、1、2
TS7~TS8	sand	25、50、100	1	1
TS9~TS10	sand	50	0.5、1、2	1
TN1~TN3	clay	25、50、100	step loading	1
TN4~TN6	clay	50	1	0.5、1、2
TN7~TN8	clay	25、50、100	1	1
TN9~TN10	clay	50	0.5、1、2	1

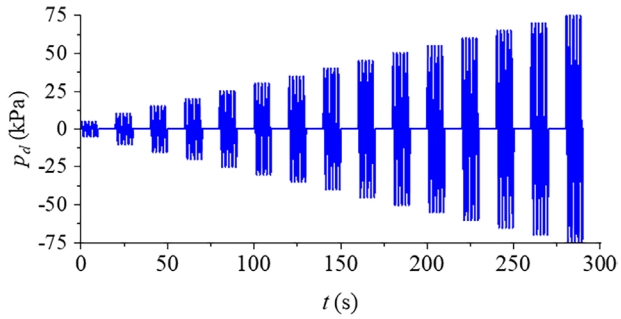

(a)

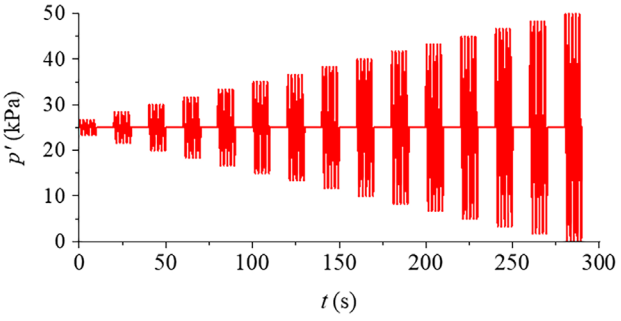

(b)

Fig. 3 Stress path (a) deviational stress, (b) effective stress

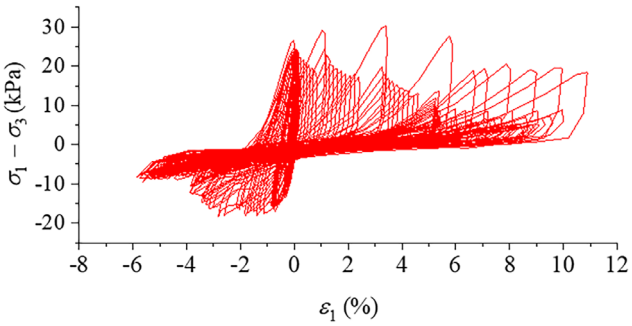

(a)

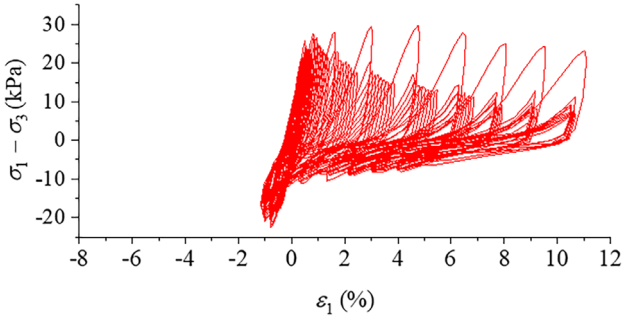

(b)

Fig. 4 Hysteretic curve (a) sand (TS1), (b) clay (TN1)

modulus (G_d) and damping ratio (λ_d) of the sample, while the cyclic loading failure test was performed to evaluate its resistance against liquefaction induced by dynamic loads.

3.1 Dynamic shear modulus and damping ratio

The stress-strain response of soil under cyclic loading exhibits typical elastic-plastic coupling characteristics. The hysteretic curve, formed due to the non-coincidence of loading and unloading paths, represents the macroscopic evolution of structural damage and energy dissipation within the material. The deviator stress ($\sigma_1 - \sigma_3$) -strain (ε) curve of the sample in the graded loading test of sand and clay is presented in Fig. 4. In these tests, confining pressure is positively correlated with the amplitude of dynamic stress. With increasing cyclic stress ratio, the hysteretic curve evolves as follows: the horizontal expansion rate of the hysteresis loop increases, the opening degree decreases, and the loop gradually deflects toward the strain axis. For sand, grain rearrangement induces significant dilatancy effects, resulting in an "S"-shaped hysteresis loop. Clay, influenced by cementation, exhibits a "butterfly"-shaped hysteresis loop.

The energy dissipation mechanism comprises two components: plastic deformation and viscoelastic deformation. Plastic deformation correlates positively with plastic strain and dominates the dissipation process when the hysteresis loop remains unclosed. Viscoelastic deformation remains approximately constant during the stable cyclic phase. The area of the hysteresis loop correlates

positively with the maximum dynamic stress. Test data indicate that the growth rate of the hysteresis area accelerates with each incremental increase of 5 kPa in CSR (10 cycles per stage). When cumulative damage reaches a critical threshold, the sample fails.

The hysteresis curve can depict the stress-strain relationship of soil materials under cyclic loading and facilitate the determination of dynamic parameters such as shear modulus and damping ratio. The dynamic shear modulus reflects the variation pattern of the stress-strain curve (backbone curve) of soil subjected to vibrational loading. The damping ratio characterizes the energy dissipation capacity of soil under cyclic loading conditions. Shear modulus and damping ratio are computed based on hysteresis loops at each load stage, with their average values representing the corresponding load stage results.

The dynamic shear modulus and damping ratio of sand samples under different confining pressures are presented in Fig. 5. It can be observed from Fig. 5 (a) that the dynamic shear modulus (G_d) of the sand sample gradually decreases with increasing shear strain. Beyond a shear strain of 0.01, there is a rapid decrease in the dynamic shear modulus, indicating that large strains lead to a reduction in soil stiffness. Consequently, under significant dynamic loads such as strong earthquakes, the soil experiences decreased stiffness, increased deformation, and heightened susceptibility to failure. Comparing results obtained under varying confining pressures reveals that higher confining pressures correspond to greater dynamic shear moduli for the samples examined. This relationship arises due to enhanced inter-particle friction resulting from elevated confining pressures, thereby leading to larger values of soil sample's shear modulus. Additionally, it can be noted that initial damping (λ) exhibited by the sand is relatively high; approximately 0.4 at a confining pressure of 100 kPa and around 0.3 at a confining pressure of 50 kPa (Fig. 5 (b)). As shear strain increases, however, the damping ratio progressively decreases until reaching approximately 0.1 during final failure stages for the sand sample investigated herein. These findings indicate that with increasing load levels, energy dissipation capacity within the sand diminishes gradually but does not become entirely depleted.

The dynamic shear modulus and damping ratio of clay samples under different confining pressures are presented in Fig. 6. The results demonstrate that the variation pattern of the shear modulus is similar to that observed in sand samples, with a gradual decrease as shear strain increases.

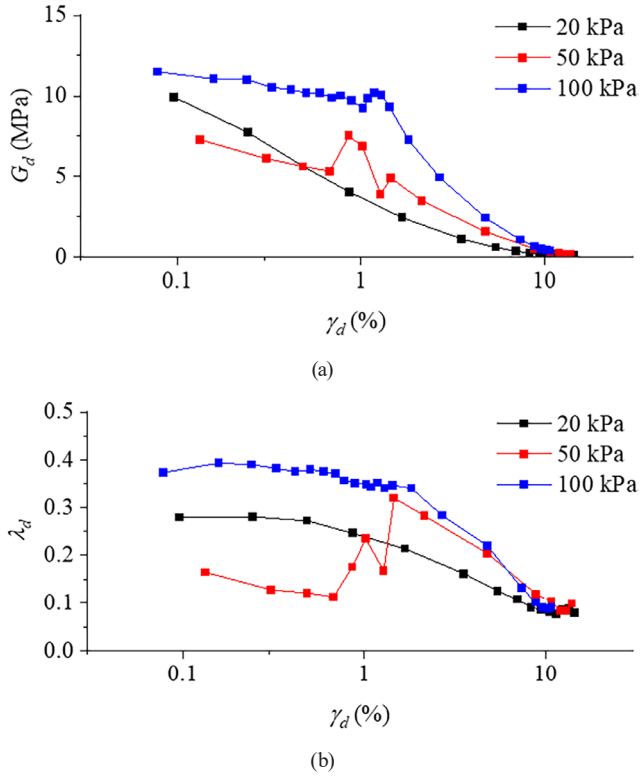

Fig. 5 Dynamic shear modulus and damping ratio of sand (a) dynamic shear modulus, (b) damping ratio

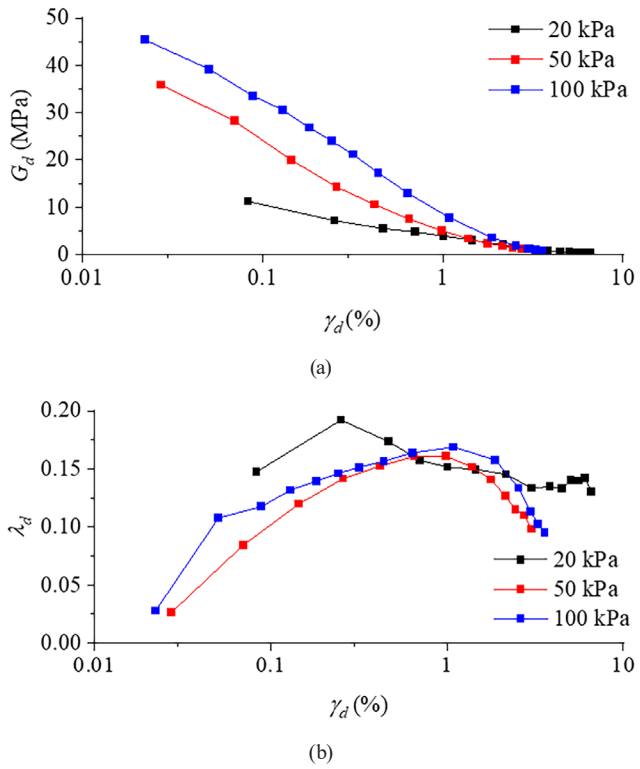

Fig. 6 Dynamic shear modulus and damping ratio of clay (a) dynamic shear modulus, (b) damping ratio

The comparison between sand and clay reveals that the dynamic shear modulus of clay surpasses that of sand due to distinct contact modes and stronger interparticle bonding forces in clay. Consequently, clay exhibits superior seismic stiffness compared to sand. However, the damping ratio of clay exhibits an initial increase followed by a decrease with increasing shear modulus due to variations in bonding modes between clay and sand particles and dissipation mechanisms under dynamic loading conditions. Furthermore, comparison between sand and clay reveals that the damping ratio of clay is lower than that of sand, suggesting better energy dissipation capacity for sand.

Sand is primarily composed of rigid minerals, such as quartz and feldspar. The particles are in point contact with one another, and the friction arises from surface roughness and normal occlusion. Under dynamic loading, sliding and rolling of particles lead to shear modulus strain softening. Clay particles exhibit a double electric layer structure, and their binding forces include van der Waals forces, electrostatic interactions, and cementation bonds. Dynamic disturbances induce recombination of the double electric layer and failure of cementation, resulting in nonlinear hysteretic responses. Natural sand forms an initially anisotropic fabric due to deposition, which becomes randomized through particle rotation and sliding under dynamic conditions. This randomization increases porosity, thereby reducing effective stress (liquefaction). Shear modulus decay and liquefaction potential are closely linked to fabric stability. Clays predominantly feature flocculated structures, and their shear modulus decreases when these structures are damaged during the initial dynamic stage. However, as strain increases, the realignment of particles can result in localized hardening, leading to a nonlinear increase in the damping ratio.

In summary, the dynamic shear modulus of sand decreases with increasing shear strain, while the magnitude of loading confining pressure positively correlates with the shear modulus. The damping ratio exhibits a decreasing trend as shear strain increases. Similarly, for clay, the dynamic shear modulus decreases with increasing shear strain and is influenced by higher confining pressures. Additionally, the damping ratio initially increases and then decreases as shear strain increases. Notably, clay demonstrates a larger dynamic shear modulus and smaller damping ratio compared to sand.

3.2 Resistance to liquefaction of soil

The dynamic strength of soil is intrinsically linked to the failure criterion. Typically, the ultimate equilibrium failure criterion, pore pressure failure criterion, and strain failure criterion are employed to assess soil failure. Among these, the strain failure criterion has emerged as the primary basis for judgment in geotechnical tests, owing to its accurate representation of progressive soil failure, strong alignment with engineering practice, and the stability of its data. Fig. 7 illustrates the number of cyclic loading cycles (N_c) for sand samples under different operating conditions when the cumulative strain reaches 5% and 10% in the cyclic loading test. The results demonstrate that, within the frequency range of 0.5 Hz to 2 Hz and with a consistent ratio between confining pressure and cyclic stress, the number of cyclic loading cycles gradually increases as the loading frequency increases during failure. Conversely, when maintaining a constant loading frequency matching the cyclic stress ratio, an increase in confining pressure leads to a decrease in cycle count. Similarly, keeping the loading frequency fixed at a specific confining pressure results in fewer cycles as deviating stress increases.

The cumulative axial strain of sand samples exhibits a transition from stable to destructive behavior as the dynamic stress increases. Moreover, an increase in vibration cycles

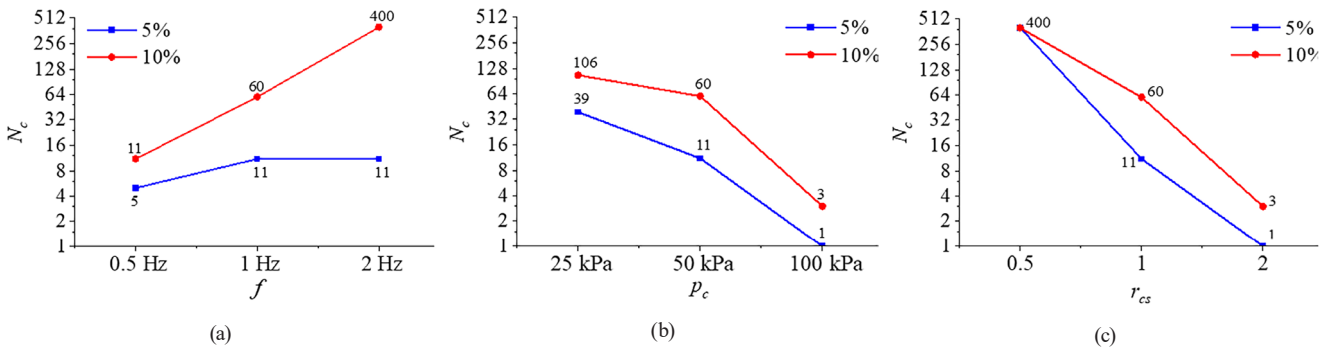

Fig. 7 Number of cyclic loading cycles for sand samples (a) loading frequency, (b) confining pressure, (c) cyclic stress ratio

leads to an enhanced inclination degree and gradual convergence of the hysteresis curve towards the stress axis, resulting in an increased resilience modulus of the soil. Additionally, there is a reduction in the area of the hysteresis ring with increasing vibration cycles, leading to its gradual linearization and a decrease in soil damping ratio, indicating pronounced elastic response. Furthermore, elevating confining pressure, dynamic stress ratio, and reducing loading frequency can expedite plastic deformation accumulation and shorten liquefaction failure time.

The cyclic loading times of the clay sample under different working conditions are shown in Fig. 8 when the cyclic loading test reaches a cumulative strain of 5% and 10%. The results indicate that within the frequency range of 0.5 Hz to 2 Hz, the number of cycles during failure initially increases and then decreases with increasing loading frequency, while keeping the ratio of confining pressure to cyclic stress constant. The failure period of clay exhibits a non-monotonic trend, initially increasing and then decreasing with the loading frequency. This non-monotonic frequency dependence is attributed to the combined effects of viscoelastic dissipation mode transformation, the coupling between pore fluid and framework, and the alignment of microscopic dynamic time scales. Moreover, when the loading frequency matches the cyclic stress ratio, an increase in confining pressure leads to a decrease in cycle count. Similarly, fixing the loading frequency at a specific value while varying deviating stress also results in a reduction in cycle count.

The increase in confining pressure of the test load enhances the inter-particle friction, thereby augmenting the sample's resistance to liquefaction. Conversely, elevating the deviational stress during testing results in a higher applied load on the sample, rendering it more susceptible to failure. By comparing the results of Figs. 7 and 8, it can be observed that the cyclic failure times exhibit consistent variation patterns for sand and clay samples under different confining pressures and deviating stresses. However, variations in loading frequencies yield different outcomes due to the distinct frequency characteristics resulting from their disparate stiffness properties. By comparing the number of cyclic failures between the two samples, it can be observed that clay samples exhibit a higher frequency of cyclic failure under identical loading conditions compared to sand. This disparity arises due to the distinct contact mode between clay particles as opposed to sand particles, resulting in stronger inter-particle bonding forces. Consequently, clay demonstrates superior resistance against liquefaction when compared to sand.

3.3 Pore water pressure growth curve

The change trend of pore water pressure in sand samples with increasing cyclic loading time (t) is illustrated in Fig. 9. As depicted, the growth curve of pore water pressure exhibits an approximate parabolic shape, and its rate gradually decelerates with increasing cycle times. When the ratio of confining pressure to cyclic stress remains constant within the range of 0.5 Hz ~ 2 Hz, a higher loading frequency leads to a faster increase in pore water pressure; however, the increment per cycle is relatively small. Similarly, when the loading frequency matches the cyclic stress ratio, an increase in confining pressure results in a faster rise in pore water pressure. Furthermore, under fixed loading frequency and confining pressure conditions, larger bias stresses lead to accelerated increases in pore water pressure along with greater amplitude for each cycle.

The change trend of pore water pressure in clay samples with increasing cyclic loading time is illustrated in Fig. 10. The growth curve of pore water pressure exhibits an approximate parabolic shape. In clay samples, the growth rate of pore water pressure remains consistent across different loading frequencies. Moreover, higher

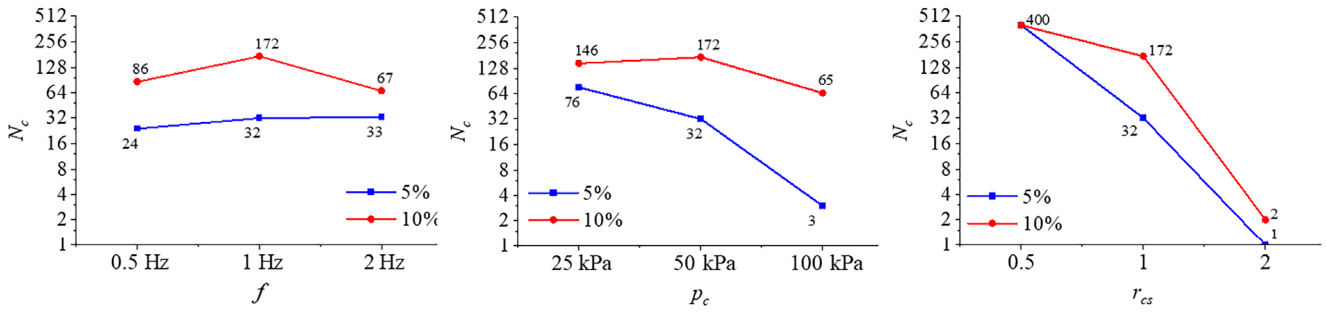

Fig. 8 Number of cyclic loading cycles for clay samples (a) loading frequency, (b) confining pressure, (c) cyclic stress ratio

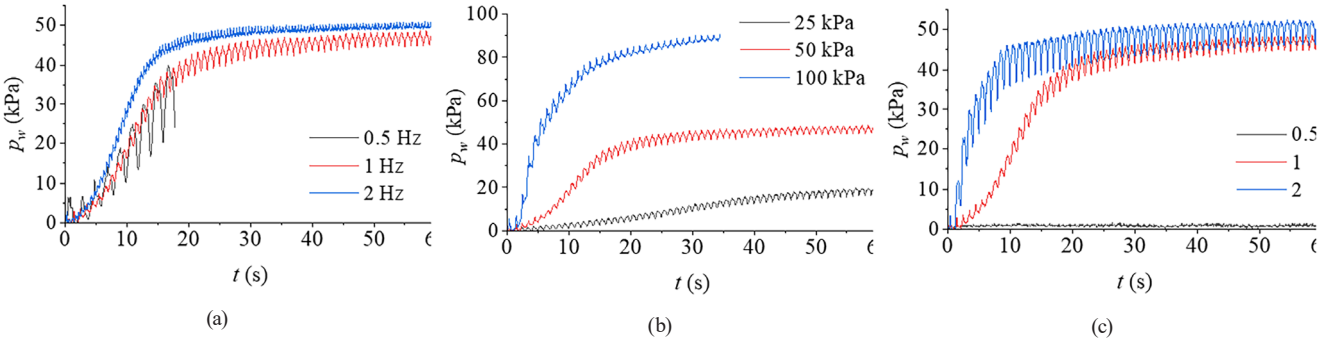

Fig. 9 Pore water pressure growth trend of sand (a) loading frequency, (b) confining pressure, (c) cyclic stress ratio

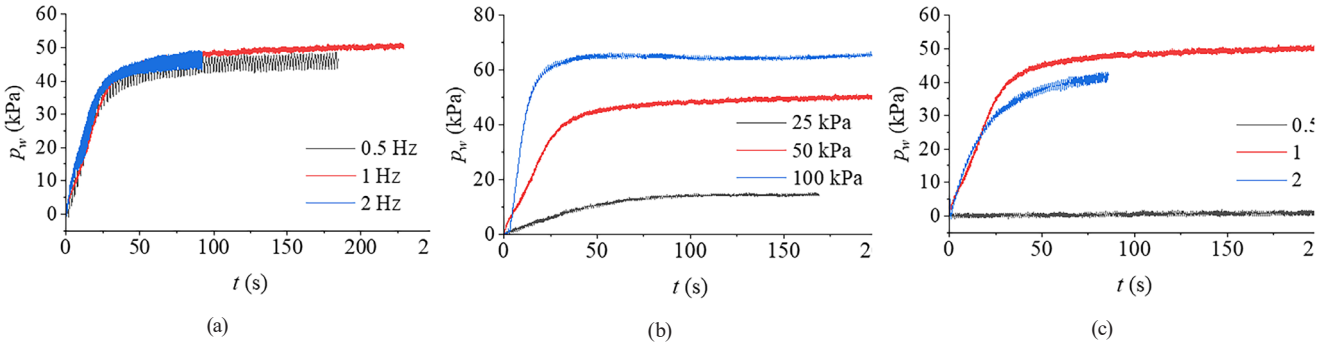

Fig. 10 Pore water pressure growth trend of clay (a) loading frequency, (b) confining pressure, (c) cyclic stress ratio

confining pressures result in faster increases in pore water pressure and greater achieved levels of pore water pressure. Notably, when the deviating stress is either 50 kPa or 100 kPa, the rate at which pore water pressure increases remains constant.

Because of the high permeability of sand, pore water pressure accumulates rapidly under dynamic loading in undrained conditions or dissipates quickly in drained conditions. This behavior directly links liquefaction risk to drainage capacity. Shear modulus attenuation is primarily governed by reductions in effective stress. In contrast, clay's low permeability makes it difficult for excess pore water pressure to dissipate, leading to a continuous decrease in effective stress under dynamic loading. However, the binding forces between clay particles, such as those from double electric layers and cementation, partially counteract the effects of pore pressure, resulting in a more gradual decay of shear modulus.

When dynamic failure occurs, the pore water pressure is presented in Table 2. The results indicate that the pore water pressure does not fully reach the confining pressure under the applied load when the specimen experiences dynamic failure.

During cyclic loading, continuous development of pore water pressure is observed in the sample. In accordance with the Moore-Coulomb criterion, effective stress decreases and the stress circle shifts towards the strength envelope. Upon reaching a critical value, pore water pressure leads to limit equilibrium state and subsequent specimen failure. The liquefaction trigger requires that the pore water pressure exceeds the effective stress. Incomplete liquefaction implies that the soil is in a partially liquefied state, where the effective stress remains positive but has substantially decreased. Even if complete

Table 2 Pore water pressure value at the time of failure

Case number	control variable	magnitude	standards of failure	
			5%	10%
TS4	f	0.5 Hz	5.27 kPa	19.09 kPa
TS5	controlled	1 Hz	19.66 kPa	47.09 kPa
TS6	f	2 Hz	28.13 kPa	/
TS7	p_c	25 kPa	14.11 kPa	21.83 kPa
TS8	p_c	100 kPa	2.14 kPa	37.20 kPa
TS9	r_{cs}	0.5	/	/
TS10	r_{cs}	2	5.62 kPa	16.58 kPa
TN4	f	0.5 Hz	5.27 kPa	19.09 kPa
TN5	controlled	1 Hz	19.66 kPa	47.09 kPa
TN6	f	2 Hz	28.13 kPa	/
TN7	p_c	25 kPa	14.11 kPa	21.83 kPa
TN8	p_c	100 kPa	2.14 kPa	37.20 kPa
TN9	r_{cs}	0.5	/	/
TN10	r_{cs}	2	5.62 kPa	16.58 kPa

liquefaction does not occur, the partially liquefied state can still result in functional failure of the engineering system. Consequently, it is necessary to integrate the strain control design concept into the relevant specifications. It can also be observed from Table 2 that higher loading frequencies result in greater pore water pressures during failure; larger loading confining pressures lead to higher levels of pore water pressure at specimen destruction; and increased loading bias stresses correspond to lower levels of pore water pressure upon specimen failure.

3.4 Dynamic characteristics of soil during liquefaction

The dynamic shear modulus and damping ratio of soil also undergo changes during cyclic loading until liquefaction failure occurs. Fig. 11 illustrates the variations in shear modulus and damping ratio of sand samples under different working conditions as the number of cycles increases. As can be seen from Fig. 11, for sand samples, the shear modulus gradually decreases with the increase of loading cycles. When confining pressure and cyclic stress ratio are consistent, the greater the loading frequency, the faster the shear modulus drops. When the loading frequency is consistent with the cyclic stress ratio, the greater the confining pressure is, the faster the shear modulus drops. When the loading frequency and confining pressure were fixed, the larger the deviational stress was, the faster the shear modulus decreased. When the deviational stress was 25 kPa, the sample did not fail, and the dynamic shear modulus of the sample did not decrease, indicating that the strength of the sample did not decrease during the loading process.

Fig. 12 illustrates the evolution of shear modulus and damping ratio curves for clay samples under varying testing conditions as the number of cycles increases. For clay samples, the decreasing trend of shear modulus remains independent of loading frequency when confining pressure and cyclic stress ratio are consistent. When the loading frequency matches the cyclic stress ratio, higher confining pressures result in larger initial shear moduli and faster declines in shear modulus. Similarly, at fixed loading frequencies and confining pressures, higher deviatoric stresses lead to lower initial shear moduli and faster decline rates of shear modulus. Notably, when subjected to a deviatoric stress of 25 kPa, the sample does not fail, and its dynamic shear modulus remains relatively unchanged.

The damping ratio curve of the sand sample under different working conditions is depicted in Fig. 13, illustrating its variation with an increasing number of cycles. The damping ratio of the sand sample gradually decreases with an increase in the number of cycles. However, this decreasing trend does not exhibit a significant correlation with the loading frequency. When the loading frequency aligns with the cyclic stress ratio, higher loading confining pressures result in larger initial damping ratios, albeit with a faster rate of decrease. Furthermore, when both the loading frequency and confining pressure are fixed, an increase in deviational stress leads to a smaller damping ratio.

Fig. 14 illustrates the damping ratio curve of a clay sample under varying operational conditions as the number of cycles increases. The results indicate that the damping ratio of clay remains relatively constant throughout cyclic loading, oscillating within the range of 0.15 to 0.2. Moreover, no significant correlations are observed between the damping ratio and factors such as loading frequency.

4 Conclusions

The triaxial vibration tests were conducted on representative sand and clay samples from the Beijing area. The study investigated the influence of various loading frequencies, cyclic stress ratios, and confining pressures on soil strength and liquefaction resistance, while also analyzing the variations in shear modulus and damping ratio. The key findings are as follows:

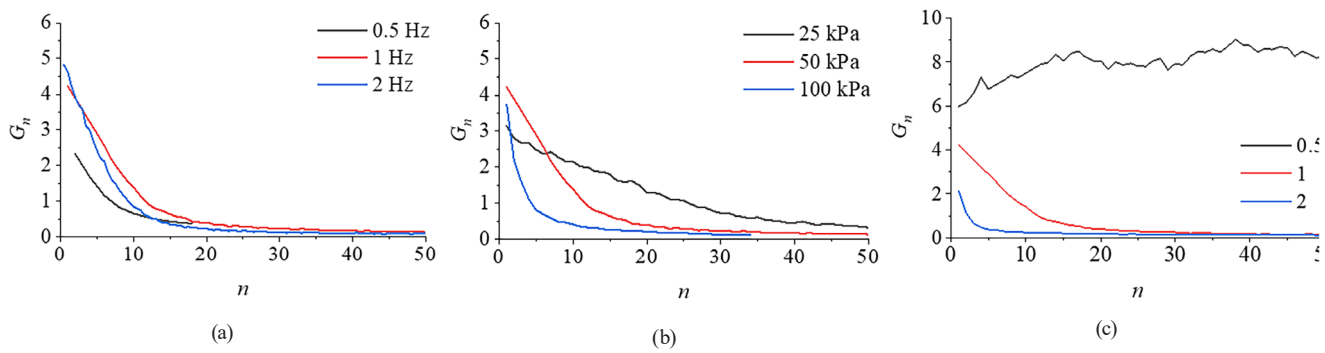

Fig. 11 Shear modulus of sand during cyclic loading (a) loading frequency, (b) confining pressure, (c) cyclic stress ratio

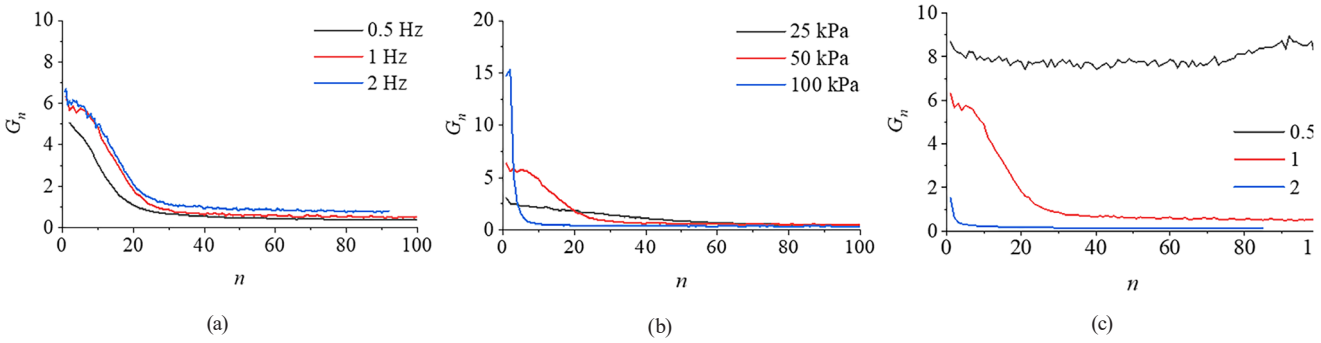

Fig. 12 Shear modulus of clay during cyclic loading (a) loading frequency, (b) confining pressure, (c) cyclic stress ratio

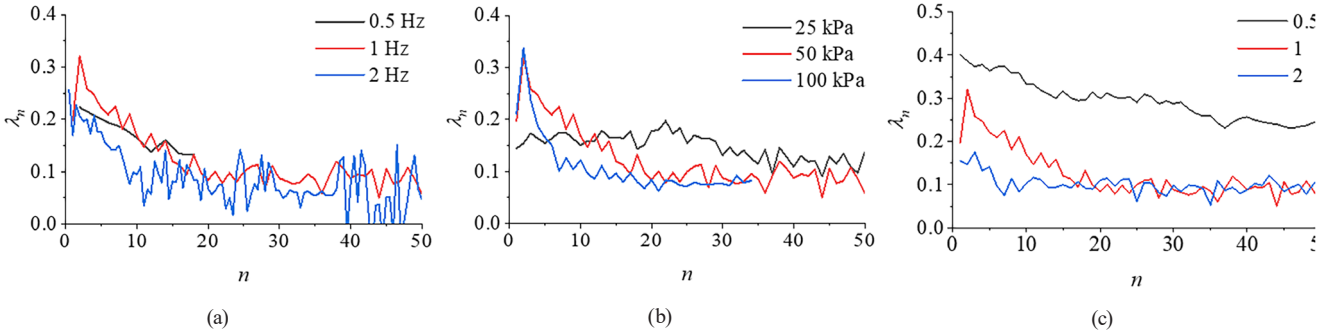

Fig. 13 Damping ratio of sand during cyclic loading (a) loading frequency, (b) confining pressure, (c) cyclic stress ratio

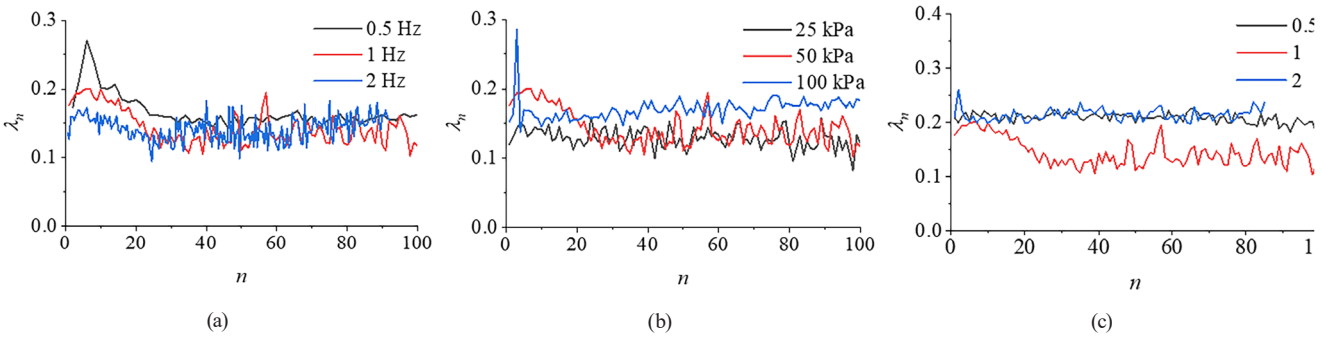

Fig. 14 Damping ratio of clay during cyclic loading (a) loading frequency, (b) confining pressure, (c) cyclic stress ratio

1. The dynamic shear modulus of sand decreases with increasing shear strain, and the magnitude of the shear modulus is larger at higher confining pressures. The damping ratio also decreases with increasing shear strain. Similarly, for clay, the dynamic shear modulus decreases with increasing shear strain, and it exhibits a larger magnitude at higher confining pressures. However, the damping ratio initially increases and then decreases with increasing shear strain. Additionally, compared to sand, clay has a higher dynamic shear modulus and a lower damping ratio.
2. The number of failure cycles decreases with increasing confining pressure and deviational stress for both sand and clay samples. However, there are variations in the results under different loading frequencies. Specifically, the cycle times of failure for sand samples gradually increase with increasing loading frequency. On the other hand, the number of failure cycles for clay samples initially increases and then decreases with increasing loading frequency.
3. The growth curve of pore water pressure follows an approximate parabolic trend. For sand samples, higher loading frequencies, greater confining pressures, and larger bias stresses lead to faster pore water pressure growth. However, no significant correlation is observed between the rate of pore water pressure growth in sand samples and either loading frequency or bias stress.
4. During cyclic loading, the shear modulus of the soil sample gradually decreases as the number of loading cycles increases. The damping ratio of sand

gradually decreases with an increasing number of cycles, whereas that of clay remains relatively stable. The variations in shear modulus and damping ratio during loading are influenced by factors such as loading frequency, confining pressure, and deviating stress.

The findings presented in this study, which pertain to the complex geological conditions in the Beijing area, necessitate parameter adjustments and technical adaptations (e.g., silicon content thresholds, vibration frequency band correction coefficients, and ecological flow allocation ratios) tailored to regional characteristics when extended to other regions or soil types. Such adaptations enable a scientifically sound extrapolation from the unique geological conditions of Beijing to other regions.

Acknowledgement
This research was funded by the Key research and development project of Chongqing Research Institute of China Coal Technology & Engineering Group (No. 2024ZDYF20) and the Innovation and Entrepreneurship Science and Technology Project of China Coal Technology and Engineering Group (No. 2023-TD-ZD014-002).

References

[1] Zhuang, H. Y. "Study on nonlinear dynamic interaction of soil-underground structure and its large-scale shaking table test", presented at GeoShanghai International Conference, Shanghai, China, June 6–8, 2006.

[2] Kesheng, Y., Ping, H., Xiaochun, D. "A discussion on the generating mechanism of 1976 Tangshan earthquake based on the geologic structure of northern Huabei Basin", Earth Science Frontiers, 17(5), pp. 263–270, 2010.

[3] Shang, S.-P., Ren, H., Zeng, Y.-L., Yu, J. "Dynamic behavior analysis of single piles embedded in nonlinear soils under vertical vibration", Gongcheng Lixue/Engineering Mechanics, 25(11), pp. 111–115, 2008.

[4] Pandya, S., Sachan, A. "Experimental studies on effect of load repetition on dynamic characteristics of saturated ahmedabad cohesive soil", International Journal of Civil Engineering, 17(6), pp. 781–792, 2019. https://doi.org/10.1007/s40999-019-00392-8

[5] Deng, G. D., Zhang, J. S., Wang, Q. Y., Shi, X., Wang, J. "Experimental research on dynamic parameters of high-speed railway coarse-grained padding", Journal of Railway Science and Engineering, 11(2), pp. 76–83, 2014. https://doi.org/10.19713/j.cnki.43-1423/u.2014.02.013

[6] Li, R. S. "Research on a new generation technique for ground seismic response analysis", Harbin. Institute of Engineering Mechanics, China Earthquake Administration, 2016. [online] Available at: https://kns.cnki.net/KCMS/detail/detail.aspx?dbname=CDFDLAST2017&filename=1016318706.nh

[7] Yang, L. G., Zhang, Y. T., Wang, H. "Experimental study of dynamic elastic modulus and damping ratio of deep clay under strain control", China Earthquake Engineering Journal, 42(01), pp. 199–204, 2020.

[8] Wang, Q., Ma, J. L., Ma, H. P., Wang, J., Wang, L. M., Gao, Z. N., Zhong, X. M., "Dynamic shear modulus and damping ratio of saturated loess", Chinese Journal of Rock Mechanics and Engineering, 38(09), pp. 1919–1927, 2019. https://doi.org/10.13722/j.cnki.jrme.2019.0249

[9] Zhao, Y. Y. "Mechanical properties of plain soils and improved soils subjected to heavy-haul train load", Harbin. Harbin Institute of Technology, 2017. [online] Available at: https://kns.cnki.net/KCMS/detail/detail.aspx?dbname=CDFDLAST2019&filename=1018897822.nh

[10] Thakur, A. S., Pandya, S., Sachan, A. "Dynamic behavior and characteristic failure response of low plasticity cohesive soil", International Journal of Civil Engineering, 19(2), pp. 167–185, 2021. https://doi.org/10.1007/s40999-020-00560-1

[11] Orense, R. P., Kiyota, T., Yamada, S., Cubrinovski, M., Hosono, Y., Okamura, M., Yasuda, S. "Comparison of liquefaction features observed during the 2010 and 2011 Canterbury earthquakes", Seismological Research Letters, 82(6), pp. 905–918, 2011. https://doi.org/10.1785/gssrl.82.6.905

[12] Yang, Z. X., Pan, K. "Flow deformation and cyclic resistance of saturated loose sand considering initial static shear effect", Soil Dynamics and Earthquake Engineering, 92, pp. 68–78, 2017. https://doi.org/10.1016/j.soildyn.2016.09.002

[13] Raihane, A., Bonnefoy, O., Gelet, J.-L., Chaix, J.-M., Thomas, G. "Experimental study of a 3D dry granular medium submitted to horizontal shaking", Powder Technology, 190(1), pp. 252–257, 2009. https://doi.org/10.1016/j.powtec.2008.04.068

[14] Johnson, P. A., Carmeliet, J., Savage, H. M., Scuderi, M., Carpenter, B. M., Guyer, R. A., Daub, E. G., Marone, C. "Dynamically triggered slip leading to sustained fault gouge weakening under laboratory shear conditions", Geophysical Research Letters, 43(4), pp. 1559–1565, 2016. https://doi.org/10.1002/2015GL067056

[15] Prasanna, R., Sivathayalan, S. "Liquefaction characteristics of sand under complex seismic loading paths", Journal of Geotechnical and Geoenvironmental Engineering, 150(10), 04024098, 2024. https://doi.org/10.1061/JGGEFK.GTENG-12046

[16] Karabulut, Z. E., Zeybek, A., Ikizler, S. B. "Particle sıze effect on the liquefactıon characteristcs of clean sand", Sādhanā: Published by the Indian Academy of Sciences, 49(4), 252, 2024. https://doi.org/10.1007/s12046-024-02592-y

[17] Nicolas, D., Alain, H. "Shear strength degradation of vibrated dry sand", Soil Dynamics and Earthquake Engineering, 95, pp. 106–117, 2017. https://doi.org/10.1016/j.soildyn.2017.01.039

[18] Seo, H., Kim, D. "Analysis of behavioral characteristics of liquefaction of sand through repeated triaxial compression test and numerical analysis", Geomechanics and Engineering, 38(2), pp. 165–177, 2024. https://doi.org/10.12989/gae.2024.38.2.165

[19] Shan, Y., Chen, T., Qiu, Z., Yuan, J., Ding, X., Cui, J. "DEM analysis of cyclic behaviors of clayey sand based on energy method", Computers and Geotechnics, 179, 107012, 2025. https://doi.org/10.1016/j.compgeo.2024.107012

[20] Zhang, Y., Lan, H., Cui, Y. "Statistical studies on shear modulus ratios and damping ratios of soil in Shanghai area", World Information on Earthquake Engineering, 26(2), pp. 171–175, 2010.

[21] Chen, G.-x., Liu, X.-z., Zhu, D.-h., Hu, Q.-x. "Experimental studies on dynamic shear modulus ratio and damping ratio of recently deposited soils in Nanjing", Chinese Journal of Geotechnical Engineering, 28(8), pp. 1023–1027, 2006.

[22] Zhan, J.-Y., Chen, G.-X., Hu, Q.-X., Yang, W.-L. "Experimental study on dynamic shear modulus ratio and damping ratio of Suzhou quaternary sedimentary soil", Chinese Journal of Geotechnical Engineering, 34(3), pp. 559–566, 2012.

[23] Zhang, X., Feng, S., Zhang, J. "Experimental study on dynamic shear modulus and damping ratio of aeolian soil in west Liaoning province", Mechanics in Engineering, 33(1), pp. 48–52, 2011.

[24] Cai, H., Jin, X. "A comparative study on dynamic damping ratio tests of structural soft soils in Fuzhou basin", Journal of Engineering Geology, 20(3), pp. 427–432, 2012.

[25] Chen, D., Tian, W., Duan, R. "Statistical study on dynamic shear modulus ratio and damping ratio of typical soils in Xi'an area", World Information on Earthquake Engineering, 28(3), pp. 136–142, 2012.

[26] Hu, Z., Luo, Y., Li, Y. "Experimental study on damping ratio variation characteristics of loess in different areas", Journal of Earthquake Engineering and Engineering Vibration, 30(2), pp. 167–172, 2010. https://doi.org/10.13197/j.eeev.2010.02.011

[27] Wang, L., Zhang, C., Li, Y., Peng, H., Fu, P., Jin, Z., Li, W. "Study on dynamic and failure characteristics of sand and anti-floating safety of tunnel structures under long-term vibration loads of the Beijing subway", Engineering Failure Analysis, 163, 108591, 2024. https://doi.org/10.1016/j.engfailanal.2024.108591